Effectiveness of Calcium Magnesium Acetate as an SO_x Sorbent in Coal Combustion

Yiannis A. Levendis, Wenqi Zhu, and Donald L. Wise
Depts. of Mechanical and Chemical Engineering, Northeastern University, Boston, MA 02115

Girard A. Simons
PSI Technology Company, Andover, MA 01810

A fundamental study was conducted on the effectiveness of the chemical calcium magnesium acetate (CMA) as a sulfur capture agent during combustion of pulverized coal. It was based on high-temperature laboratory-bench experiments with the scope of exploring the use of CMA as a "dry scrubbing" medium for in-boiler injection. Two methods of CMA introduction in the furnace were considered: dry-spraying fine powders of the chemical and wet-spraying aqueous solutions to generate fine aerosols. It considered conditions pertinent to post-flame in-boiler injection of CMA to identify optimum temperatures and residence times. In addition to the versatility of the water-soluble CMA to enable spray drying injection and therefore eliminate grinding costs, there are other attractive features. Mainly, its ability to form highly cenospheric, "popcorn"-like, oxide particles on heating to high temperatures. These cenospheres possess thin, porous walls with blowholes that enable penetration of the SO_2 in the interior of the particle which promotes high sorbent utilization. SO_2 captures in the order of 90% were achieved with dry-injection of the chemical at furnace gas temperatures of about 1,000°C, a Ca/S ratio of 2, and particle size of $\approx 50\ \mu m$. Moreover, CMA was superior (by over 40%) to either $CaCO_3$ or $Ca(OH)_2$ in sulfur capture effectiveness per unit mass of calcium. This commercially obtained CMA was even superior to reagent-grade calcium acetate (by as much as 30%), again per unit mass of calcium. The utilization of CMA and calcium acetate depended on the cenosphere wall thickness, rather than the particle size and, thus, outperformed other sorbents regardless of the size of the resulting oxide particles.

Introduction and Literature Review

Gaseous sulfur emissions, predominantly SO_2, from combustion of coal can be controlled through heterogeneous reactions with sorbents to form stable sulfur-containing solids. Criteria for the selection of the sorbent include: effectiveness, availability, cost, and stability of the products of sulfation. Extensive experimental work has shown that calcium compounds, such as limestone, are effective sulfur scavengers in gasification and combustion (Case et al., 1973; Chang et al., 1986; Sharma et al., 1987; Togan et al., 1989).

To comply with current Clean Air Act Amendments and resulting environmental regulations, control of sulfur emissions in coal-burning power plants is presently achieved by post-combustion flue gas wet scrubbing using calcium compounds. Despite their high sulfur removal efficiencies, such installations involve high capital investment and operating costs. Moreover, wet scrubbers suffer from severe corrosion and plugging problems.

Alternative cleanup technologies introduce calcium compounds in the combustion or post-combustion region of power plants and are termed "dry scrubbing" since the product of sulfation is solid. These technologies incorporate both dry-spraying powders and wet-spraying slurries of the sorbent. Typical sorbents are various forms of calcium carbonate ($CaCO_3$), calcium hydroxide ($Ca(OH)_2$), dolomite ($CaCO_3$-$MgCO_3$), hydrated dolomite, sodium based (Nahcolite $NaHCO_3$, and Trona Na_2CO_3-$NaHCO_3$-$2H_2O$) as well as other

mixed cation compounds (Muzio and Arand, 1981). The products of sulfation of sodium based sorbents, however, are water soluble and may leach to groundwater after disposal in landfills, thus creating another experimental problem. Sorbent-spraying techniques are easy to implement and require small capital cost but are moderately effective with 30–70% SO_2 removal (Amrnhein et al., 1992; Stouffer and Yoon, 1990).

Injection of sorbents can be allocated in the furnace, in the post-furnace zone or the exhaust ducts (in the presence of water). Selection of the optimum place for injection is dictated by thermodynamic and kinetic processes. Temperature, residence time and SO_2 concentration influence the effectiveness of the sorbent. For effective heterogeneous reactions the sorbent should be small in size, porous and well dispersed in the combustion effluent gases.

Upon injection in a high-temperature environment (>700°C), sorbents consisting of calcium compounds (and magnesium compounds) undergo *calcination* or decomposition to CaO (and MgO). The density of CaO is higher than that of its precursors (for example, $\rho_{CaO}/\rho_{CaCO_3} = 1.22$) thus, during this step the porosity and internal surface area increase drastically. For instance, Borgwardt (1985) reported that during calcination at 1,100°C the BET surface for calcium carbonate and calcium hydroxide powders grew from a few m^2/g to 80 m^2/g and porosities reached 60%; calcination for 10 μm particles was measured to be 70% complete in 0.1 s.

At a little higher temperatures, 1,000–1,200°C, the phenomenon of *sintering* or "deadburning" may take place, the pore structure collapses, and the calcium oxide particles rapidly lose porosity and internal surface area (Borgwardt, 1985; Borgwardt, 1989; Garman and Munir, 1976; Simons and Garman, 1986). Loss of more than 35% of surface area has been reported, in simultaneous calcination and sintering experiments when the temperature was increased from 1,012 to 1,152°C (Mai and Edgar, 1989). Thus, sintering appears to impose an upper limit to the temperature range that is suitable for sorbent injection. However, it is encouraging to note that Borgwardt et al. (1984) have reported that the rate of sintering is rather slow at least at intermediate temperatures, taking 10 min at 1,000 K (727°C).

Finally, in the presence of SO_2 or H_2S gas a third process takes place simultaneously with the previous two: *sulfation*. During this process, CaO reacts with the gases to form solid sulfate, sulfite or sulfide mainly by the following two reactions:

$$H_2S + CaO \rightleftharpoons CaS + H_2O \quad (1)$$

$$CaO + SO_2 + \frac{1}{2}O_2 \rightleftharpoons CaSO_4 \quad (2)$$

under reducing and oxidizing conditions, respectively. The reactions occur in the internal pore structure or grains of the CaO particles, not just on the external surface. At very high temperatures or low enough sulfur concentrations, the reverse of reactions (1) and (2) take place and gaseous sulfur products are re-released. If this phenomenon occurs, any benefits of sorbent injection are lost. The rate of sulfation is high in the temperature range of 900–1,200°C (Simons, 1988). The fact that this is the same temperature window where sintering takes place simultaneously renders the analysis of the overall process very challenging. Moreover, the formation of $CaSO_4$ from CaO increases the solid volume by a factor of 3.3. Thus, if the particle does not expand upon reaction, the amount of $CaSO_4$ formed in the pores is determined by the pore volume. Hence, for a porosity of 50% only a little over 50% of the CaO can be converted to $CaSO_4$ (Flagan and Seinfeld, 1988).

Mathematical models that describe SO_2 retention by porous CaO, in the absence of sintering, have been developed such as "pore models" (Calvelo and Cunningham, 1970; Batia and Perlmuter, 1983; Yortsos and Sharma, 1984; Simons et al., 1986, 1987; Yu and Sotirchos, 1987) "grain models" (Szekely and Evans, 1970, 1971; Sohn and Szekely, 1972, 1973; Szekely and Propster, 1975) or "overlapping grain models" (Lindner and Simonson, 1981; Sotirchos, 1987; Sotirchos and Yu, 1988).

This work used the pore model of Simons (1986, 1987, 1988) for comparison with experimental results. In this model the mechanistic description of the process includes the pore structure, pore branching, species transport, reaction kinetics, product deposition, pore filling, pore plugging and diffusion through the product layer. Results of this model have shown that small-pore filling is dominant for 1- to 10-μm-dia. particles, while pore mouth plugging is dominant for 100-μm to 1-mm-dia. particles. The most important parameters influencing the sulfation process were found to be the sorbent particle size, the porosity, the total surface area and the particle temperature-time history (cooling rates). The dependence of the sulfation rate on temperature and SO_2 concentration is given by Simons (1988), in the absence of sintering. For instance, in an effluent stream containing 4% O_2 and 3,000 ppm of SO_2, $CaSO_4$ is expected to be unstable above $\approx$1,210°C (1,483 K), and the maximum rate of sulfation (Reaction 2) is predicted to occur at a temperature around 1,150°C (1,423 K), but at 300 ppm the maximum rate would occur at 1,070°C.

Gullett and Bruce (1987) and Bruce et al. (1989) conducted experimental studies comparing the sulfation rates of CaO particles derived from either $CaCO_3$ or $Ca(OH)_2$ and found the latter to be more reactive. This was attributed to the slit or plate-like pore structure of the hydroxide-derived CaO, vs. the cylindrical or spherical pores of the limestone-derived CaO. Bortz et al. (1986) reported that precalcination of the sorbents does not promote utilization.

There has been some disagreement in the literature regarding the mechanism that controls the sulfation reactions, however, there appears to be an overall consent on the range of the intrinsic activation energy, 30–34 kcal/mol (Simons et al., 1987).

Finally, related work by Lynch and Elliot (1978) and by Torres-Ordoñez et al. (1989) on the oxidation of CaS(s) in O_2-SO_2-Ar atmospheres and temperatures between 1,180 and 1,580°C, indicated that reaction of CaS to CaO and/or $CaSO_4$ happened in layers, the outside layer transforming to CaO and the core remaining CaS. Also, Ibarra et al. (1989) analyzed coal ashes, obtained at low temperatures and concluded that only the outer layers of the calcium oxide were active in sulfur retention. From these findings it appears that the chemical transformation in the solid sorbent may occur in onion-like layers, the depth and composition of which varies with particle size, surface porosity, particle temperature, oxygen partial pressure and residence time.

From the above it becomes obvious that the heterogeneous reaction of CaO (a solid) with SO_2 (a gas) depends on the available surface area of the solid, thus small particle size,

high porosities and internal surface areas, as well as existence of large "feeder" pores and, if possible, hollow (cenospheric) particles are desirable. Only then the SO_2 gas will be able to penetrate the interior of the solid sorbent particle, not just the outside layers. This will provide for high sorbent utilization (conversion to the sulfated product) and will minimize sorbent waste and, thus, associated costs.

Although there is a large amount of work reported in the literature on calcium based sorbents, little is known about the effectiveness of either Calcium Magnesium Acetate (CMA) or Calcium Acetate (CA) as in-boiler or post-combustion sorbents. (The only difference between CA and CMA is in the magnesium content, the latter being produced from dolomitic stone. The magnesium itself, however, is not expected to react with SO_2 to any significant degree at high temperatures.) The unique property of CMA and CA to calcine forming highly cenospheric CaO particles of superior physical structure has been identified in this work. Furthermore, CMA and CA being highly soluble in water (up to 30 and 37% by mass, respectively, at room temperature) (the solubility of $CaCO_3$ is only 0.0015% and that of $Ca(OH)_2$ is 0.18%) provide the unparalleled flexibility of introducing them in the furnace by either all-dry or wet-spraying techniques. The experiments described herein aim at investigating the behavior of sorbent particles that are generated either by dry- or wet-spraying of CMA and CA.

Experimental Results

Experimental apparatus and procedure

Experiments were conducted in a high-temperature, drop-tube furnace, by bringing together an SO_2 containing gas and dispersions of sorbent particles. Known quantities of these reactants were introduced at the top of the furnace and the products of reaction were monitored at the bottom. Four different sorbents were used herein for comparative purposes: CMA ($CaMg_2(CH_3COO)_6$), CA ($Ca(CH_3COO)_2$), calcium carbonate ($CaCO_3$), and calcium hydroxide ($Ca(OH)_2$). The CMA was commercially available from Cryogenic Technologies, with 95% purity; the rest were of chemical reagent grade, purchased from Aldrich. SO_2, balanced in N_2, was purchased from Matheson. Both wet-sprayed and dry-sprayed CMA were examined.

The experimental apparatus used is described as follows:

High-Temperature Laboratory Furnace. A high-temperature, drop-tube, laminar flow furnace, capable of heating a 25 cm long, alumina radiation cavity to temperatures up to 1,650°C, was used for this work. The length of this cavity is nearly isothermal. Injection of sorbent particles was conducted through a stainless steel water cooled injector, mounted at the top of this furnace, Figure 1. Furnace and injector gas flows were regulated to provide for a variety of SO_2-N_2-O_2 mixtures controlled by electronic mass-flow meters.

Furnace wall temperatures were continuously monitored by type B thermocouples attached to the wall. Gas temperatures inside the furnace were measured, at various axial and radial positions, by a specially constructed *suction thermometer*. In this instrument the furnance gases were forced to flow isokinetically around a shielded thermocouple junction and through a permeable blanket. Gas temperature and velocity profiles were also calculated through detailed numerical modeling, using the *Fluent* software and gas residence times were so obtained (Cumper et al., 1990).

The sorbent powders were introduced at the top of the furnace injector using a *particle fluidizer*, shown in Figure 1. A glass vial containing sorbent particles (bed) is advanced by a constant velocity syringe pump, while a slender tube (leading to the furnace) is held inserted into the vial. A constant air flow is used to entrain the particles from the top of the bed and carry them into the tube. The entrance of the tube is beveled and is always kept half-immersed in the receding surface of the particle bed. The vial and the tube are vibrated to facilitate fluidization.

Droplet Generators. To facilitate the study of wet-sprayed particles of CMA, equal size drops of aqueous CMA solutions were produced using a droplet generator (Levendis and Flagan, 1989a,b). This instrument induced a high frequency vibration on a steady-flow of solution as it was forced through a small orifice (pinhole). Under certain conditions the liquid jet was broken up into monodisperse droplets, whose size was controlled by the width of the orifice, the oscillator frequency and the liquid feed rate. The vibrations were induced by a piezoelectric element driven by a function generator. These droplets were not sprayed directly in the furnace, but instead, they were dried first in a thermal reactor resulting in solid particles in the range of 40–60 μm. Upon collection of the particles from the reactor they were dry-sprayed in the furnace. This procedure was necessitated by physical constraints in the furnace that did not provide sufficient time for water evaporation from droplets in the generated size range.

Thermal Reactor. A stainless steel, down-flow, thermal reactor (1.5 m high, 10.1 cm ID) was used for the precalcination experiments with wet-spraying of CMA. The droplet generator was mounted at the top of this reactor, where provisions were incorporated for introduction of gas streams, to disperse and dilute the droplets (Levendis and Flagan, 1989a). Fixtures for viewing the droplet stream as well as testing for monodispersivity, *in situ*, have been encompassed in the design. Dry sorbent particles were collected at the bottom of this reactor.

Experiments with wet-spraying water solutions of CMA *directly* in the furnace was accomplished using fine particles only. These micron-size particles were generated using two small *nebulizers* connected in parallel, Figure 1, and were thereafter conducted, as an aerosol, to the furnace.

Experimental Procedure. Sulfation experiments were conducted in the high temperature furnace at gas temperatures in the range of 750–1,150°C. The SO_2 partial pressure in the incoming gas was 550 ● 10 ppm the balance was 89% N_2 and 10.5% O_2. Molar calcium to sulfur ratios of 1 (stoichiometric) and 2 were used. The gas flow rate in the furnace was constant (at STP); thus, the residence time increased with decreasing gas temperature.

The sorbent particles were conducted to the furnace by a fluidizer at constant air flow rate, Figure 1. The effluent gas from the furnace was passed through two gas-washing bottles in series, containing a solution of 1% H_2O_2 (Chang et al., 1986), Figure 1. In this medium SO_2 was converted to H_2SO_4, the amount of which was determined by titration. Blank runs were executed by passing SO_2 containing gas at the absence of sorbent in order to determine the amount of SO_2 absorbed by the furnace walls (alumina). The amount of SO_2 absorbed reached steady state after $\approx$ 1.5 h, hence experiments were run succeeding this period. The results of blank runs served as a baseline for the sorption experiments.

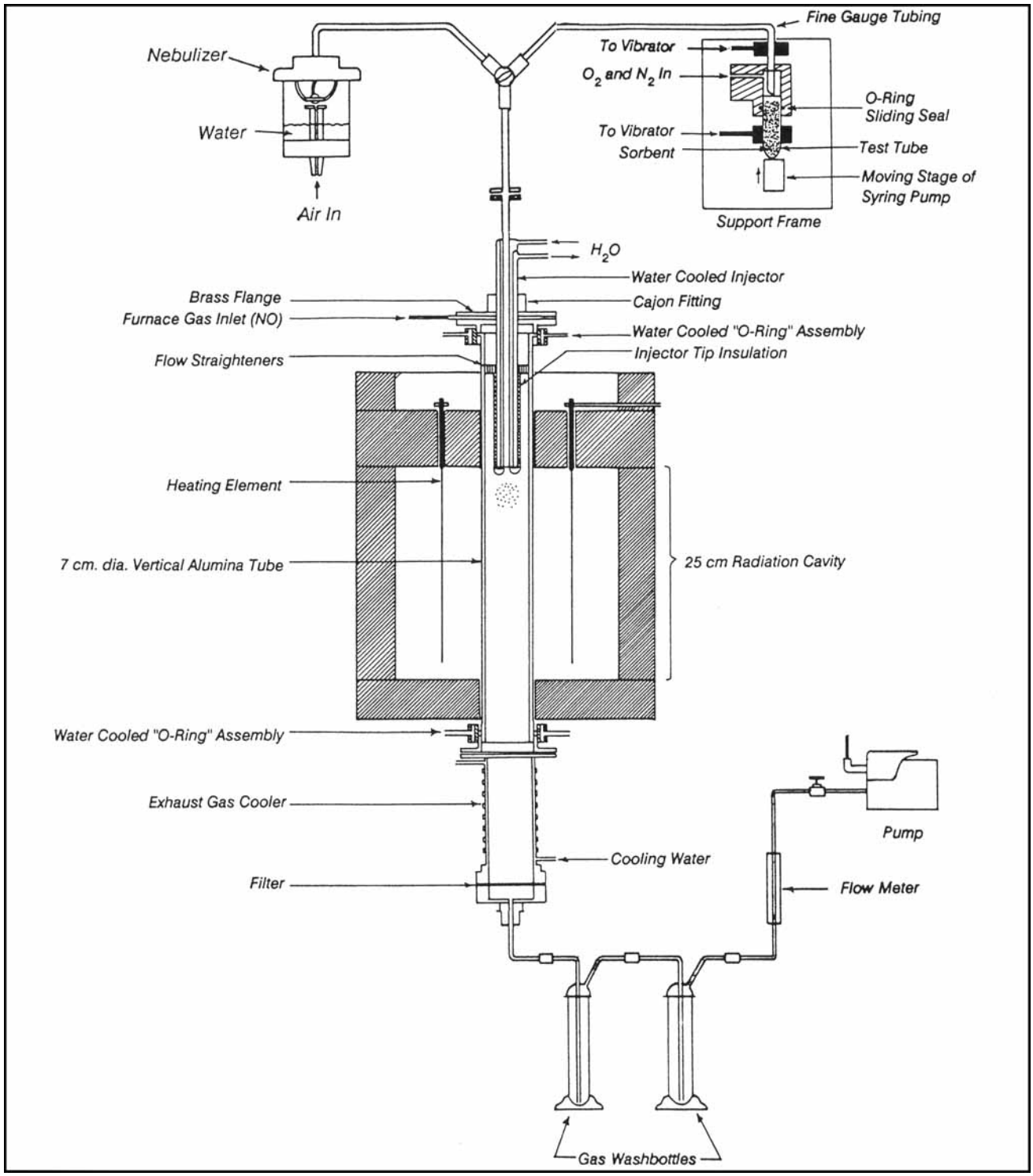

Figure 1. Externally heated, laminar flow furnace and associated experimental apparatus.

The total (internal and external) surface area of the particles was measured by N_2 adsorption at 77 K in a standard BET apparatus (at Northeastern University). Apparent density and true density of selected samples were measured by mercury porosimetry and helium pycnometry, and porosity and pore-size distributions were deduced by both mercury porosimetry and N_2 capillary condensation (at Micromeritics). The particles were also examined by X-ray fluorescence to identify the calcium and magnesium concentrations and by X-ray diffraction to identify the chemical composition.

High-temperature calcination of CMA

As mentioned earlier, the fact that CMA and CA are orders

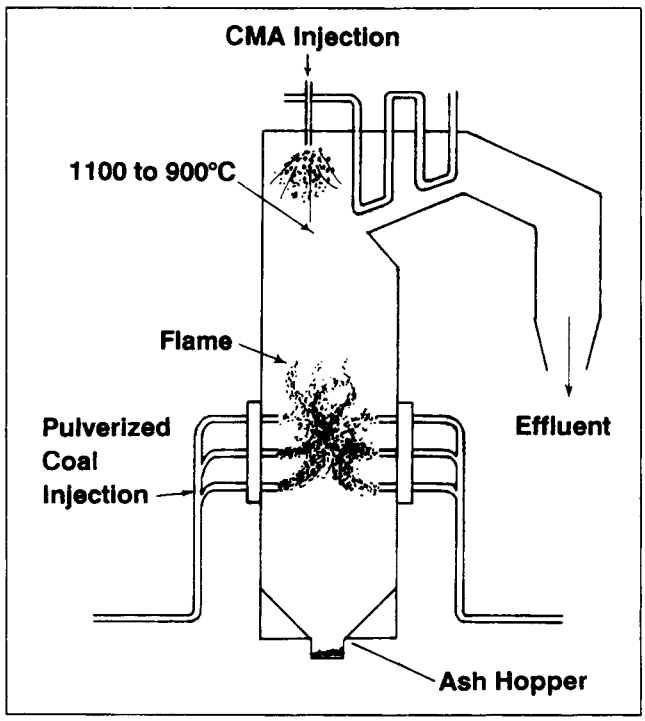

Figure 2. Possible CMA injection location in the post-flame zone of a boiler.

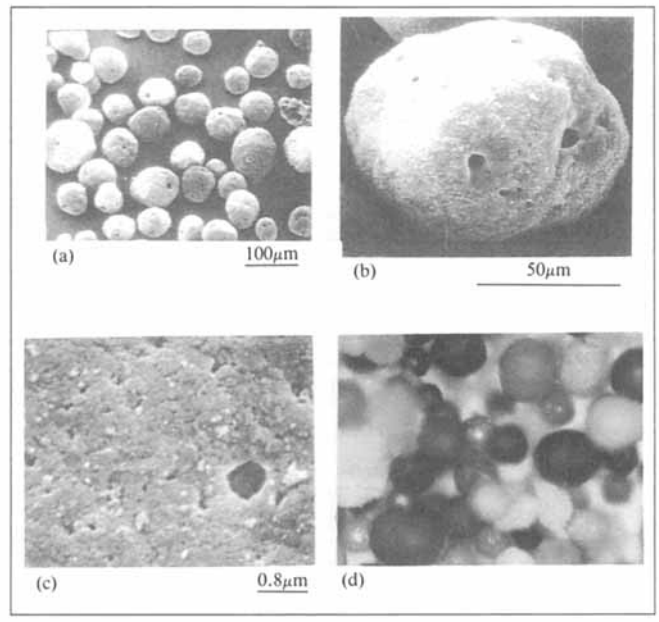

Figure 4. (a) and (b) SEM photographs of CMA particles, similar to those of Figure 3 after dry-spraying in air, at 1,150°C and a residence time of 4-5 s; (c) high magnification SEM reveals the structure of the matrix; (d) an optical microscope photograph of the same material.

of magnitude more soluble than other calcium-based sorbents, such as $CaCO_3$ or $Ca(OH)_2$, provides the flexibility of injecting these sorbent in the furnace either by (a) dry-spraying a powder or (b) wet-spraying aqueous solution of these compounds. The latter technique can eliminate the cost of grinding the sorbent to fine particles. Furthermore, CMA (or CA) can be injected either in the furnace or in the post-combustion zone, Figure 2.

In all experiments, performed herein, it was very interesting to find out that both CMA and CA, heated at high temperatures, using either of the above spraying techniques, resulted in highly cenospheric particles resembling "popcorn"-like structures.

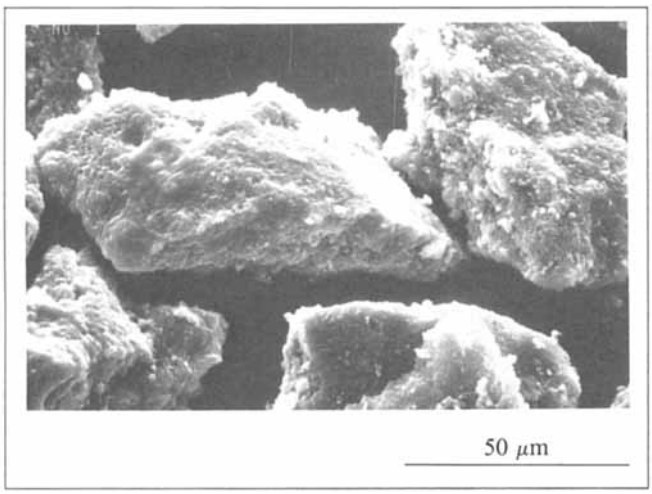

Figure 3. SEM photographs of CMA particles ground to 45-53 μm size.

CMA was obtained from Cryogenic Technologies.

Dry Spraying Experiments. CMA was ground by mortar and pestle and sieve-classified. Particles in the size range of 45-53 μm are shown in Figure 3. Such particles were then placed in vials (test tubes), weighted, and fluidized in air and, thence, introduced to the high temperature drop-tube furnace. In Figures 4a-4d the calcined product (CaO and MgO) of these particles is depicted after passing through the furnace at T_g of 1,150 K and a residence time in the order of 4 s. These oxide particles are highly cenospheric with thin porous walls (4-10 μm) pierced with large blowholes (a few microns in diameter). These large pores may serve as SO_2 feeder-pores to the interior of the cenospheres and improve sorbent utilization. While Figures 4a-4c are SEM micrographs, the photograph on Figure 4d was taken with an optical microscope. This picture shows a rather unexpected particle to particle color variation, ranging from bright yellow to brown, gray, black, and so on.

Wet Spraying Experiments. Oxide particles have been produced by spray drying an aqueous solution of CMA at a temperature of 600°C in air, Figure 5. To produce these particles a solution of 5 wt. % CMA in a water-acetone (50-50) mixture was conducted to an aerosol generator and sprayed in a thermal reactor. In the reactor, upon evaporation of the liquid, the CMA decomposed to calcium and magnesium oxides. The aerosol generation technique was controlled to produce particles of similar size (Panagiotou and Levendis, 1991). The produced particles were also cenospheric with thin and porous walls, as evidenced by a few that were deliberately crushed, Figure 5. These particles were quite fragile. Finally, these particles were passed through the high temperature furnace at T_g of 1,150°C. No visible morphological changes were induced

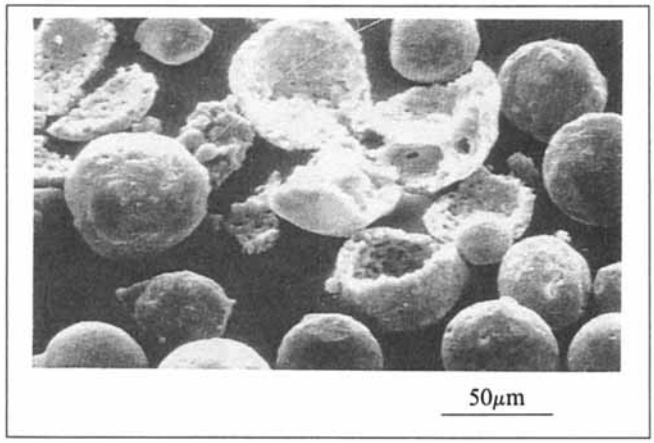

Figure 5. (a) SEM photographs of CMA particles, generated by a wet-spraying technique in air, at 600°C and a residence time of 4-5 s.

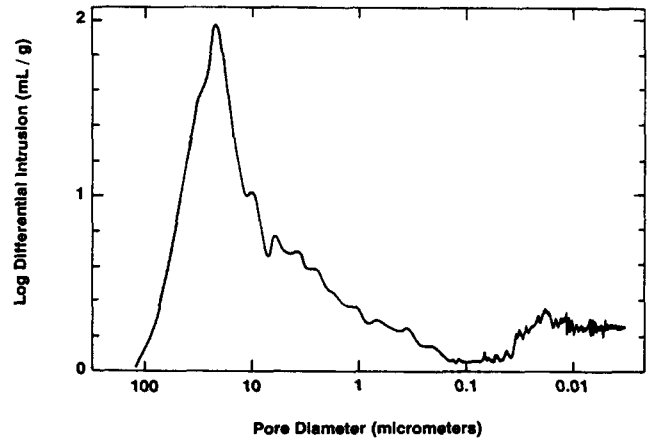

Figure 6. Mercury intrusion pore-volume vs. pore size for CMA particles, 45-53 μm, dry sprayed in air at 1,000°C (1,273 K) and a residence time of 4-5 s (Case 1).

to the particles, during this additional heat treatment and the particle to particle color variation remained unaltered. SEM X-ray fluorescence on individual particles revealed that the magnesium to calcium ratio was ≈2.

The most important feature of these sorbent particles, thus, appears to be their cenospheric nature which can enhance the utilization of the oxide by facilitating diffusion to the interior. Comparative results for two representative cases of sorbents generated by the above techniques are given below.

Properties

Case 1: dry-sprayed, 1,000°C, air, ≈50 μm particles

BET area = 27 m^2/g
ρ_{bulk} = 0.81 g/cm^3
$\rho_{skeletal}$ = 2.20 g/cm^3
ρ_{helium} = 2.38 g/cm^3
Porosity = 66%
Cumulative pore volume = 2.23 cm^3/g
Cumulative pore volume in macropores, 50 nm$<d<$2 μm = 0.29 cm^3/g
Cumulative pore volume in mesopores, 2$<d<$50 nm = 0.27 cm^3/g
Cumulative pore volume in micropores, $d<2$ nm = not measured.

Case 2: wet-sprayed, 1,000°C, air, ≈50 μm particles

BET area = 35.2 m^2/g
ρ_{bulk} = 0.66 g/cm^3
$\rho_{skeletal}$ = 2.90 g/cm^3
ρ_{helium} = 2.92 g/cm^3
Porosity = 77%
Cumulative pore volume = 2.16 cm^3/g
Cumulative pore volume in macropores, 50 nm$<d<$2 μm = 0.47 cm^3/g
Cumulative pore volume in mesopores, 2$<d<$50 nm = 0.29 cm^3/g or 0.136 cm^3/g (measured by N_2 capillary condensation)
Cumulative pore volume in micropores, $d<2$ nm = not measured.

The above porosities are estimated to be those of the particle shell, excluding the central void of the cenospheres. Corresponding pore-volume and pore-surface vs. pore-size distributions are shown in Figures 6-9. Figure 6 represents the differential mercury intrusion volume, plotted against the pore diameter, for the sample of Case 1 (dry-sprayed). The large and wide peak in the region of 10-50 μm corresponds to the large interior voids of the particles (some have more than one) and possibly to interparticle space. Thus, when calculating the porosity of the cenosphere wall, any pores bigger than the diameter of the surface blowholes (≈5 μm) were disregarded. Also, a large concentration of pores was detected in the neighborhood of 0.01 μm. A similar plot for Case 2 (wet-sprayed) is shown in Figure 7. There are three distinct peaks in this pore distribution. There is a large and narrow peak centered at ≈15 μm indicative of multiple intraparticle voids in these sorbents (in contrast to the dry-sprayed particles, most of which include one void). A second rather distinct hump encompasses pore sizes in the range of 1-3 μm. These pores were also detected by SEM, Figure 5a. Finally, a third peak can be observed in

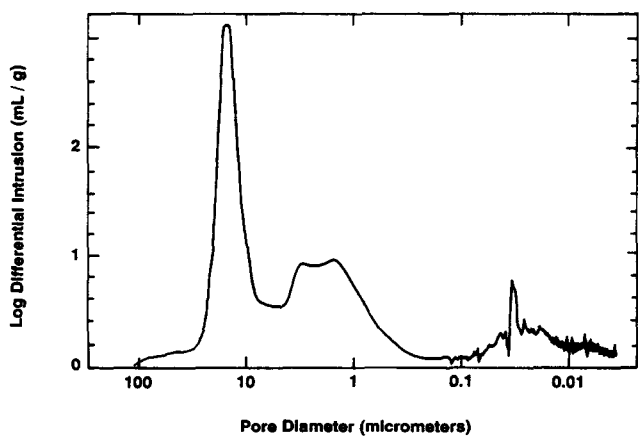

Figure 7. Mercury intrusion pore-volume vs. pore size for CMA particles, 45-53 μm, wet-sprayed in air at 873 K and then treated at 1,273 K in air for 4-5 s (Case 2).

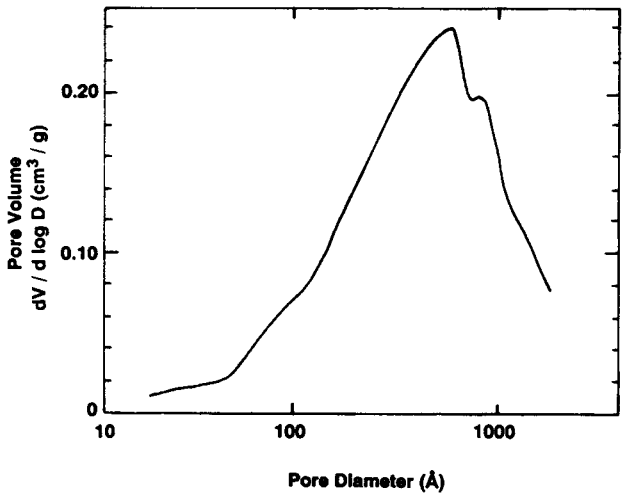

Figure 8. N_2 adsorption pore-volume vs. pore size for CMA particles, 45–53 μm, wet-sprayed in air at 873 K and then treated at 1,273 K in air for 4–5 s (Case 2).

the neighborhood of 0.03 μm (300 Å), that is, mesopores. To verify the presence of such mesopores, N_2 capillary condensation measurements were performed in this sample (wet-dryed). Figures 8 and 9 depict the pore-volume and the pore-surface distributions of the adsorption part of the isotherm for this sample, respectively. It can be noticed that, indeed, this technique detected a large concentration of pores in the size range of 0.03–0.08 μm (peak at 0.07 μm), which is close to the range detected by mercury porosimetry. Smaller pores were also detected, as attested by the dual peaks (30 and 100 Å) in the pore surface area plot of Figure 9. These pores (small meso-pores) account for most of the surface area. Thus, the trimodal pore structure of the cenosphere walls of these sorbents has the potential of facilitating pore diffusion of SO_2 and heterogeneous reaction (sulfation).

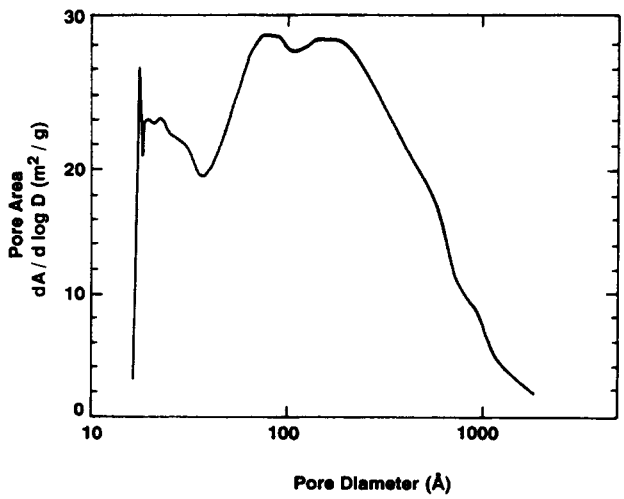

Figure 9. N_2 adsorption pore-surface area vs. pore size for CMA particles, 45–53 μm, wet-sprayed in air at 873 K and then treated at 1,273 K in air for 4–5 s (Case 2).

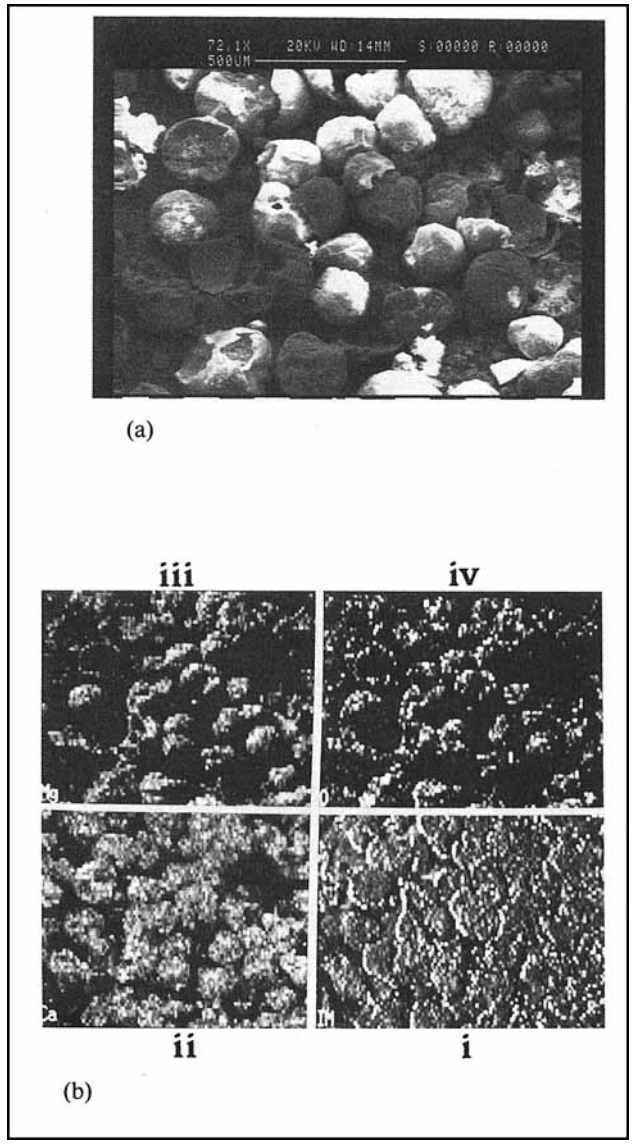

Figure 10. (a) SEM photograph of CMA-derived oxide particles (dry-spraying); (b) EDX mapping of the same sample; clockwise from right side bottom: (i) image, (ii) Ca, (iii) Mg and (iv) O.

Chemical characterization

Chemical characterization was performed with energy-dispersive X-ray (EDX) techniques, using a Kavax, Leica SEM, and with X-ray diffraction (XRD) techniques. A sample of calcined CMA (CASE I, above) was partially crushed, Figure 10a, and examined for the presence of the elements Ca, Mg, and oxygen. The results of the EDX mapping are shown on Figure 10b, where all three elements appear to be present in every particle. Other impurities, such as iron, were not detected. Hence, the variability in color among the CMA-derived oxide particles may not be attributed to mineral impurities, rather it may be the result of the formation of calcium and magnesium suboxides. Visual observation of the sulfated sorbents revealed that samples treated at a gas temperature, T_g, of 750°C appeared light gray in color, similar to the predom-

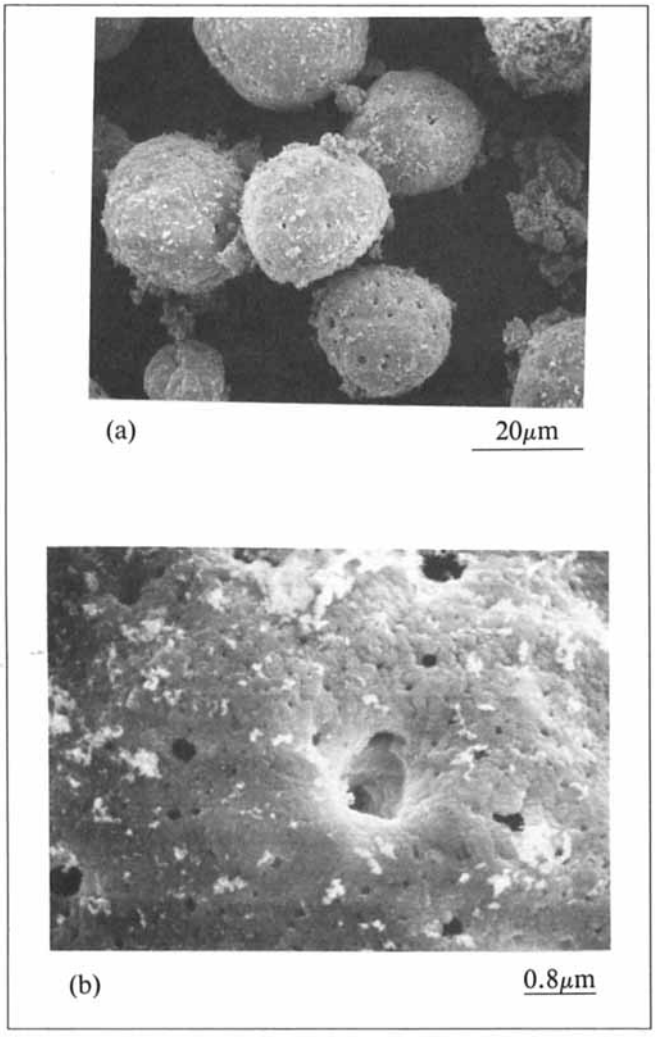

Figure 11. (a) SEM photograph of sulfated CMA particles; (b) high magnification SEM reveals the structure of the matrix.

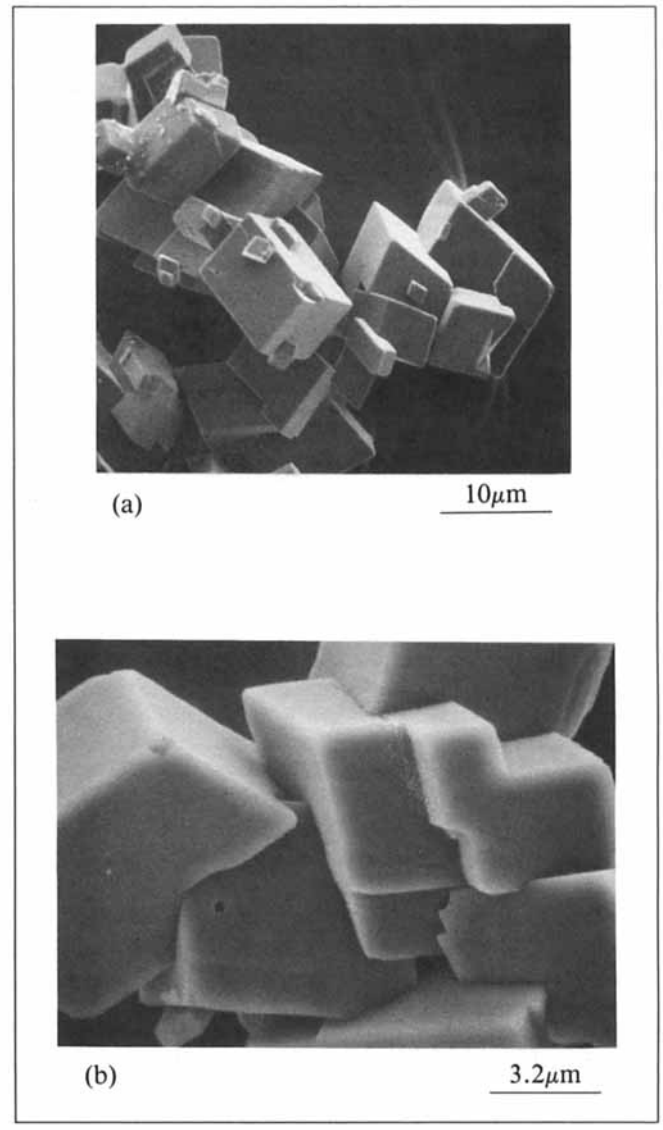

Figure 12. SEM photographs of (a) calcium carbonate particles; (b) calcium carbonate particles after sulfation, at 950°C, 4.5 s.

inant color of the oxide percursor. The samples that were sulfated at higher temperatures possessed progressively lighter, ivory-like colors.

Results of the XRD analysis revealed CaO and MgO peaks in the calcined sorbents as well as in those sulfated at low temperatures. $CaSO_4$ peaks were evident in all sulfated sorbents. Neither $CaSO_3$ nor $MgSO_4$ peaks were detected. SEM micrographs of CMA particles after sulfation at T_g of 950°C, Ca/S = 2, are shown in Figure 11.

Other sorbents examined

For comparative purposes, three other sorbents were commercially purchased from Aldrich: calcium carbonate ($CaCO_3$), calcium hydroxide (Ca(OH)) and calcium acetate ($Ca(CH_3COO)_2$). SEM micrographs of calcium carbonate particles, before and after sulfation, are shown in Figure 12; they are crystal cubes in the size range of 5–10 μm. Calcium hydroxide particles, before and after sulfation, are shown in Figure 13; they are multilayered crystals with dimensions around 5 μm. Visual examination of the SEM micrographs revealed that sulfation caused mild size expansion, rounding of surfaces and removal of sharp edges and laminations. Calcium acetate (CA) particles are shown in Figure 14; they are needle-shaped crystals 5–10 μm long and a fraction of 1 μm wide. Upon calcination and sulfation, however, these particles formed cenospheric structures, either individually or a few particles combined (fused) together, Figures 14b and 14c.

Sulfur capture experiments

The sulfur capture effectiveness of the above sorbents, dry-sprayed in the furnace, was studied at various temperatures and two calcium/sulfur molar ratios (1 and 2). Results are shown in Figures 15 (Ca/S = 2), and 16 (Ca/S = 1) where the sulfur removal by the different sorbents was plotted vs. gas temperature. It should be kept in mind here that the reactor length was isothermal during these experiments and the SO_2 concentration in the gas was 550 ppm. Furthermore, it should

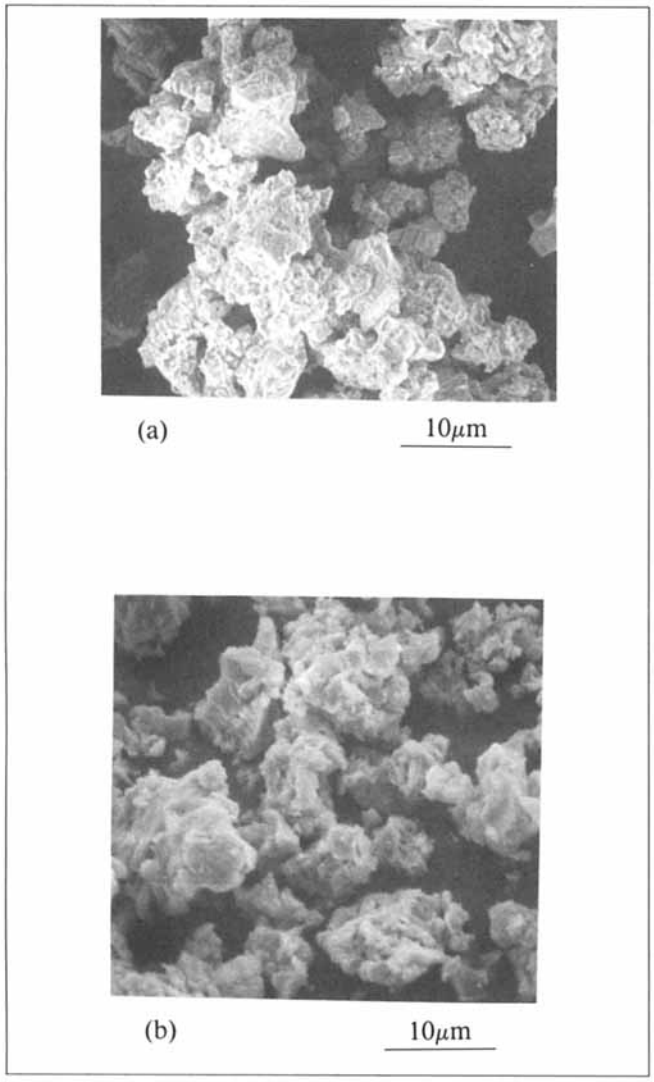

Figure 13. SEM photographs of (a) calcium hydroxide particles, (b) calcium hydroxide particles after sulfation, at 950°C, 4.5 s.

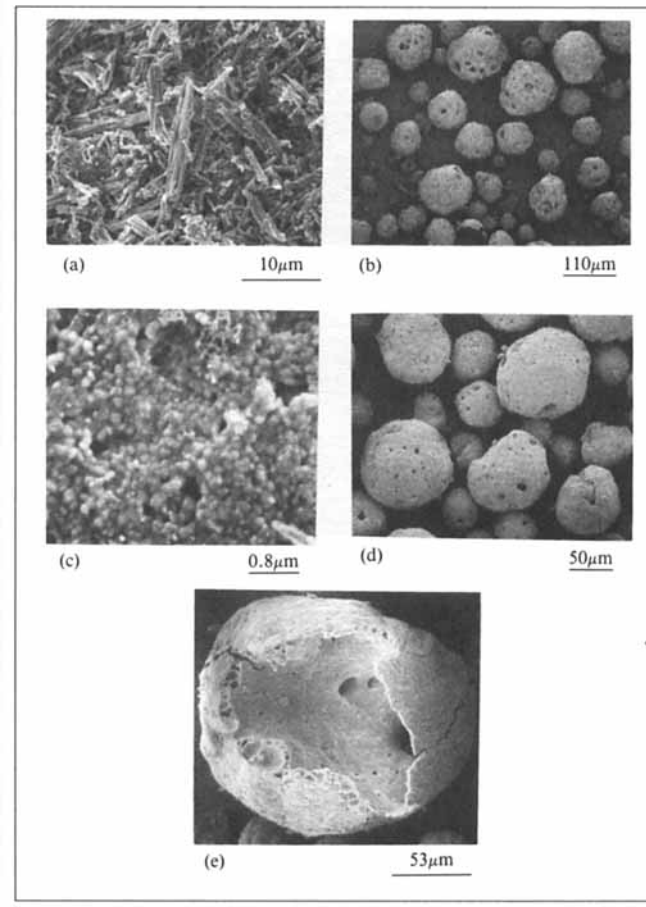

Figure 14. SEM photographs of (a) calcium acetate (CA) particles; (b) CA particles after calcination, at 950°C, 4.5 s; (c) same under high magnification; (d) CA particles after sulfation, at 950°C, 4.5 s; (e) same under high magnification.

be noted that the gas temperatures, T_g, were approximately 50°C lower than the wall temperatures, T_w, and the estimated sorbent particle temperatures were between T_g and T_w. Reaction was assumed to take place at the particle temperature.

For a Ca/S ratio of 2, Figure 15, maximum sulfur removal efficiencies were achieved at furnace gas temperatures in the range of 850–1,050°C (1,123–1,323 K). Since, at this Ca/S ratio, the amount of calcium introduced is two times that required for stoichiometric reaction the sorbent conversion to $CaSO_4$ (termed sorbent utilization) is half the amount of the removed sulfur. From these results it can be seen that CMA was the most effective sorbent, reaching efficiencies as high as 91% at T_g of 950°C (1,223 K). The effectiveness of calcium acetate (CA) was found to be lower, approximately 50–55% at the above temperature. Both calcium carbonate and calcium hydroxide performed in the 30–40% region, the hydroxide being a little better. The experiments at T_g of 950°C (1,223 K) were repeated four times resulting in a ±5% scatter in the data. This can be attributed to unsteady fluidization and dispersion, as well as loss of the sorbent in the particle feeder lines and the injector. Therefore, the upper values in each spread of data correspond to situations where particle fluidization and dispersion was effective, and thus, are indicative of the potential of the technique in turbulent flow furnaces.

It can be noticed that the sulfur removal effectiveness of CMA and CA reached a maximum around T_g of 950°C and thereafter, the effectiveness decreased at higher temperatures. However, based on theoretical kinetic calculations (Simons, 1988), at the concentration of 550 ppm used in these experiments, the maximum sulfation rate should be expected to occur at ≈1,080°C (1,350 K). The fact that the observed maximum rate temperature is lower than that theoretically predicted may be due to mild effects of sintering. This is supported by measured BET surface areas, which also followed a similar trend with temperature and exhibited a peak around 950°C, Figure 17.

In the case of Ca/S ratio of 1, Figure 16, maximum sulfur removal efficiences were achieved at furnace gas temperatures again in the range of 850–1,050°C (1,123–1,323 K). This Ca/S ratio is the stoichiometrically correct for the sulfation reaction, hence, the mole fractions of the calcium utilization and

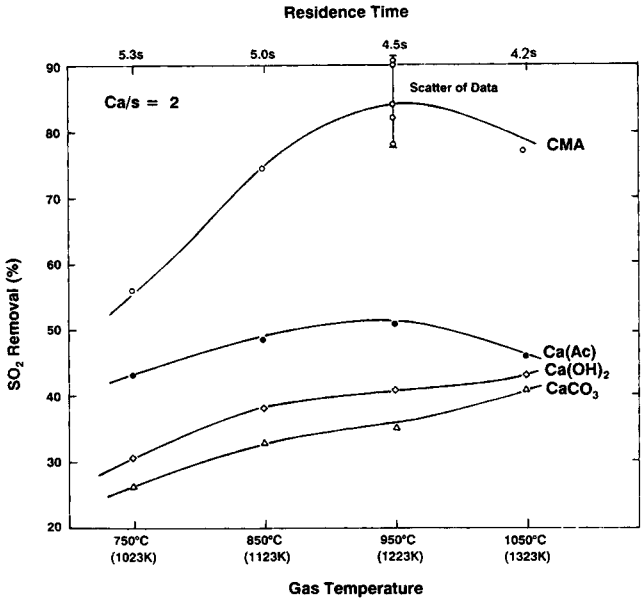

Figure 15. Experimental results on the SO_2 removal vs. gas temperature for CMA (50 μm), calcium acetate (1 x 5 μm), calcium carbonate (5-10 μm) and calcium hydroxide ($\approx$5 μm) at a Ca/S ratio of 2.

the sulfur removal are equal. CMA was again the most effective sorbent per unit mass of calcium, 10-20% more effective than the rest, achieving calcium utilizations in the range of 50%.

It is anticipated that even higher calcium utilizations would have been obtained if: a) The axial profile of temperature in the experimental furnace was nonisothermal, that is, if the temperature decreased with the SO_2 concentration (Simons, 1988, Figure 2); b) the experimental furnace was nonlaminar, that is, if better particle dispersion was provided. Since actual

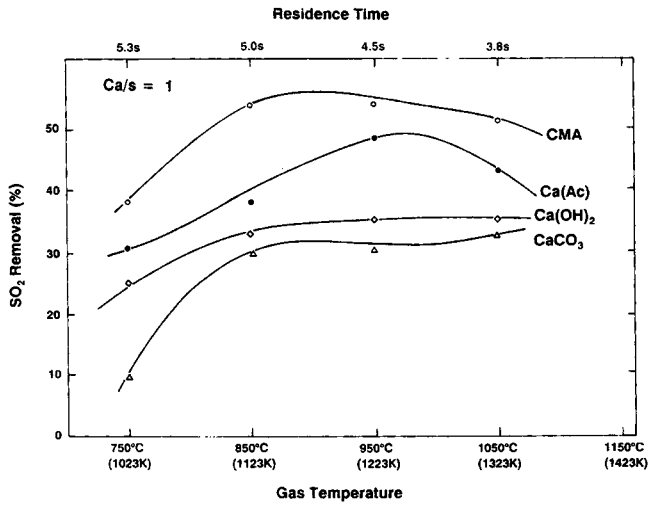

Figure 16. Experimental results on the SO_2 removal vs. gas temperature for CMA (50 μm), calcium acetate (1 x 5 μm), calcium carbonate (5-10 μm) and calcium hydroxide ($\approx$5 μm) at a Ca/S ratio of 1.

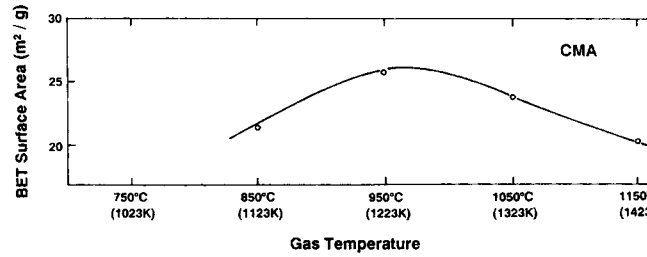

Figure 17. BET surface area of CMA-derived (CaO·*m* MgO) particles (50 μm) calcined at various temperatures.

furnaces are turbulent with strong cooling gradients, it is expected that calcium utilization will improve further; and c) very small particles were generated, even smaller than the cenosphere wall thickness (4-10 μm). Such micron-size particles were produced with nebulization of CMA or CA solutions in water and are shown in Figure 18. Experiments were conducted at Ca/S = 0.2, at T_g = 950°C. The sorbent utilizations were estimated, within experimental error, to be close to 100%.

Unfortunately, there is no present major supply of calcium magnesium acetate. While calcium magnesium acetate is also being investigated as a noncorrosive deicing salt (Bungay and Hudson, 1987) the cost is still high due to the expensive acetate and not to the cost of lime, which is plentiful in the U.S. Acetate is currently produced in pilot-plant quantities from acetic acid, made from natural gas and fermentation of by-products of food industries. On the other hand, parallel research at Northeastern University is investigating the production of calcium magnesium acetate from renewable organic or "biomass" substrates and sewage sludge (Bungay and Hudson, 1987; Wise and Augenstein, 1988; Wise et al., 1991) so that the cost of this material will be drastically reduced.

To minimize the cost of CMA sorbent injection, it may be practical to implement a dual injection scheme, that is, a combination of in-boiler injection of CMA (at Ca/S ratio of 1) and in-duct injection of lime-water slurries. Furthermore, to reduce the actual weight of the sorbent that is introduced in the furnace, CMA with low magnesium content should be used as a sulfur capture agent. To investigate this further, a series of combustion experiments with CMA of various contents of

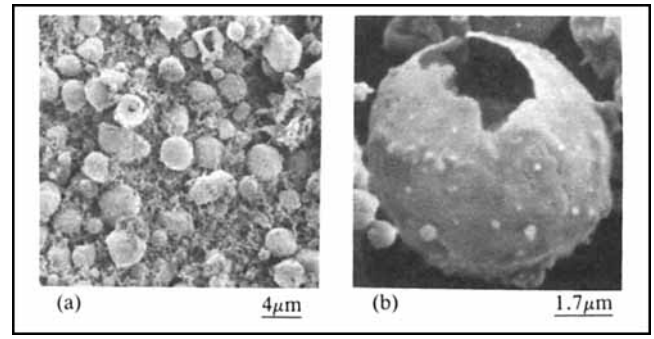

Figure 18. (a) SEM photographs of CMA particles, generated by nebulization of a water solution, at 950°C; (b) high magnification SEM reveals the structure of the matrix.

Table 1. Sulfation Model Parameters

Material	Molar Vol. (cm^3/mol)	Molar Wt. (g/mol)	Density (g/cm^3)
MgO	11.26	40.3	3.58
CaO	16.9	56.1	3.32
$CaSO_4$	52.1	136.1	2.61
(CaO·*m* MgO)	16.9+11.26*m* (39.4 for *m*=2)	56.1+40.3*m* (136.7 for *m*=2)	$\left(\frac{3.32+2.38m}{1+0.665m}\right)$ (3.46 for *m*=2)
($CaSO_4$·*m* MgO)	52.1+11.26 *m* (74.62 for *m*=2)	136.1+40.3 *m* (216.7 for *m*=2)	$\left(\frac{2.61+0.773m}{1+0.216m}\right)$ (2.902 for *m*=2)

magnesium are planned in the future to assess the role of magnesium. CMA with high magnesium content should be used as a deicing salt since, in this application, magnesium plays the most important role.

Analysis and Discussion of Results

The experimental results on the sulfur removal effectiveness of CMA particles have been contrasted to theoretical calculations based on a computationally simple, physics-based model (Simons, 1988). [The model predictions were computed based on physical data (porosity, surface area, and so on) obtained for CaO derived from CMA; they may be also valid for CaO derived from CA. Both of these calcium oxides, derived from acetate compounds of calcium, were highly porous. Since physical data for the less porous calcium oxides derived from either $CaCO_3$ or $Ca(OH)_2$ were not obtained in this study, the corresponding experimental results were not compared with theory.] This approach of contrasting theory and experiments can greatly enhance our understanding of the data, notably reduce the amount of data that must be taken, and suggest the most important regions of parameter space in which to collect data. The CMA (or CA) transformation may be broken into three distinct steps:

- Atomization of the water/CMA (or CA) solution, in the case of wet-spraying method
- Droplet dehydration and formation of the porous oxide sorbent
- Sulfation by the porous sorbent.

Only the last step was examined in this investigation. The pore structure model employed herein is known as the pore tree

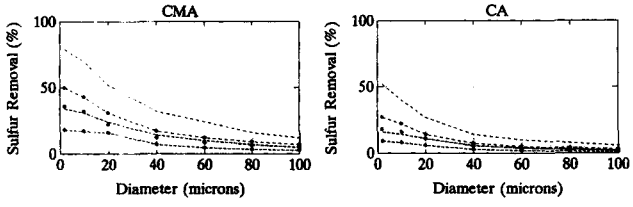

Figure 19. Model predictions of SO_2 removal at various particle sizes and temperatures of (a) CaO·*m*MgO and (b) CaO, Ca/S ratios of 1 and 2, 550 ppm SO_2.

The porosity was 60% and BET areas in the neighborhood of 25 m^2/g, as given in the text. (a) (·—·—·—) 1,050°C; (b) (····) 950°C); (c) (----) 850°C. Curves with asterisks (*) denote Ca/S ratio of 1.

(Simons, 1988). The sorbent pore structure is described as a set of trees whose trunks are located at the particle surface and the branches in the interior. The distribution of pores of radius r_p is proportional to $(1/r_p)^3$. The transport equations include the effects of bulk diffusion to the particle exterior surface, continuum diffusion within the large pores, and Knudsen diffusion within the small pores. The model corrects for these processes and accounts for first-order chemical kinetics at the pore walls. The forward intrinsic rate constant, k_s was expressed in an Arrhenius form $k_s = 6\times10^4$ kg/(m^2 s MPa) $\exp(-17{,}000/T)$. The reverse reaction rate was also accounted for, with the expression $k_s' = k_s(1-p_v/p_s)$, where p_s is the local SO_2 pressure and p_v is the equilibrium vapor pressure given by $p_v = 10^{12}/\sqrt{p_{O_2}}$ MPa $\exp(-52{,}000/T)$ with p_{O_2} in kPa. This pore structure/pore transport model yields the reactivity as a function of temperature and time, and includes the effects of product deposits, that is, the increased molar volume of $CaSO_4$ over that of CaO.

Sulfation modeling used the following initial structural data for the calcite generated by dry-spraying at 1,273 K (CASE 1 above): porosity of 66% and the temperature-dependent BET surface area data of Figure 17. To idealize the sulfation of these calcium-based salts, the calcine sorbent is considered to react as if the magnesium were inert. Thus, (CaO·*m* MgO) + SO_2 + 1/2O_2 → ($CaSO_4$·*m* MgO) where *m* relates to the molar ratio of Mg/Ca. For the degenerate case (*m*=0), the model of Simons and Garman (1986) describes the sulfation of CaO. However, for CMA the molar volumes and densities of the reactants and products must be determined. These parameters alter the rate and extent to which the pores of the calcined CMA are filled with sulfate. These values are listed in Table 1 and are readily implemented into the model. The intrinsic rate constant was not altered, although subsequent findings may suggest it is appropriate to do so.

The model parameters in Table 1 immediately suggest an increased calcium utilization for CMA. Notice that the molar volume during sulfation of CaO increases by a factor of 3.1, thus, plugging the pores and limiting conversion. However, the molar volume during sulfation of (CaO·*m* MgO) increases by a factor of only 1.9. This permits better utilization of the oxide.

Theoretical results are shown in Figure 19, where the predicted percent of sulfur removal is plotted vs. the sorbent particle diameter, in the range of 2 to 100 μm, furnace gas temperatures in the range of 1,023–1,323 K, 550 ppm SO_2 and Ca/S ratios of 1 and 2. Figure 19b is pertinent to CaO, meanwhile Figure 19a corresponds to CMA-derived (CaO·*m* MgO), with *m*=2 for the CMA compound used herein. As expected, the SO_2 removal effectiveness of both types of sorbents decreases, inversely proportional to the sorbent particle size. Furthermore, the effectiveness improves with increasing temperature in this range. It can be seen, from Figure 19d, that the predicted SO_2 removal efficiency of CMA at 950°C, Ca/S=2 and a particle diameter of 50 μm is 25% instead of the measured efficiencies in the range of 80–90%. Keeping in mind that the model approximates the physics of solid particles and not cenospheres, this discrepancy could be explained by the fact that the SO_2 gas penetrates the interior of the cenosphere where reaction also takes place. (The penetration of SO_2 to the interior of the cenosphere may not be complete because of pore diffusion limitations.) Thus, the effective

thickness of the particle may be equal to the cenosphere walls, that is, 4–10 μm, where the model actually predicts close to 90% sulfur removal. Thus, the CMA-derived sorbent outperforms the calcium carbonate and calcium hydroxide sorbents because of its superior cenospheric structure. To explore this point further, additional sulfation experiments were conducted using three different CMA particle size cuts:

- 125–150 μm
- 53–62 μm
- 38–45 μm

All of these batches formed cenospheric particles upon calcination and/or sulfation, the latter occasionally combining together to form large "pop-corn"-like particles with comparable wall thickness. Sorbent particles in all of these size cuts resulted in sulfur removal efficiencies in the low to mid-80% region at Ca/S = 2 and 950°C. Thus, as revealed by the theoretical analysis, the wall structure and thickness, rather than the particle size, are the important parameters in assessing the utilization of the cenospheric sorbent particles (CMA and CA). The wall thickness of the cenospheres, produced herein, was in the range of 4–10 μm which might have been subjected to mild pore diffusion limitations. In contrast, micron size particles, that were, indeed, produced by the nebulization of CMA or CA solutions, Figure 18, seem to react in a kinetically control regime, free of pore diffusion limitations. Associated sorbent utilization was measured to be close to 100%, as predicted by the model.

Furthermore, there may be additional advantages of the dolomite-derived CMA over the calcite-derived CA, attributed to its pore structure and shape of the pores, as suggested elsewhere (Cole et al., 1986), but most importantly to the smaller increase of the molar volume of the sulfated product. Thus the likelihood of plugging of pores during sulfation is less in CMA than in CA. Finally, there is a possibility of catalytic action of impurities, like iron, and so on, that are present in the commercially available CMA.

The model reproduced the SO_2 removal data obtained at high temperature (above 850°C) for all sorbents but underpredicted somewhat the data at the lowest gas temperature. This effect cannot be attributed to the magnesium since it is not present in three of the sorbents. However, the model was fully validated (Simons et al., 1987) only in the SO_2 partial pressure range of 60 Pa to 5 kPa and the present database is below 56 Pa SO_2. Since SO_2 goes through several intermediate steps to form $CaSO_4$, the rate limiting step at low SO_2 pressure and low temperature may have a lower activation energy and/or reaction order than that determined at high SO_2 pressure. This will be investigated further in a future study as it is important in achieving greater than 80% SO_2 removal in standard combustion systems, that is, in obtaining less than 600 ppm SO_2.

Conclusions

The results of this investigation showed that Calcium Magnesium Acetate (CMA) appears to be a superior SO_2 sorbent for in-boiler injection. This, however, was calculated per unit mass of the calcium content and not per unit total mass of the sorbent (including magnesium). Hence, to minimize the unnecessary waste of the magnesium, CMA with low magnesium content should be used in coal combustion. CMA with high magnesium content should instead be utilized as a deicing salt where it excels. Due to their special cenospheric structure, calcinated CMA particles with thin and porous walls (4–8 μm) outperformed calcium carbonate, calcium hydroxide and even calcium acetate (CA) particles of much smaller physical dimensions. Large blowholes on the surface of CMA-derived CaO provided important SO_2 pathways to the intraparticle space, which facilitated reaction and resulted in high sorbent utilization. Sulfur removal efficiencies as high as 90% were recorded with a Ca/S ratio of 2. It is expected that even higher efficiencies will be obtained in turbulent gaseous streams containing higher SO_2 aided by better mixing of the sorbent with the gas and by gradually cooling the effluent.

The fact that CMA performed better than CA per mole of calcium can be attributed to reduced likelihood of pore plugging during sulfation because of the smaller relative increase in the molar volume of the products in the presence of magnesium, the larger overall mass of CMA introduced in the furnace at a constant Ca/S ratio, and thus the resulting better fluidization and dispersion, and possibly, better physical structure, that is, thinner walls of the CMA cenospheres. It should be mentioned here that Cole et al. (1986) reported that sorbents derived from dolomitic limes performed better than those derived from calcitic limes. That finding may be explained again using the former of the arguments above, as well as on the basis of a more favorable pore structure/shape and possible resistance to sintering.

Finally, the SO_2 removal effectiveness of dry-sprayed CMA particles as well as of predried and then dry-sprayed CMA particles of similar size was comparable. Thus, in these experiments the role of water vapor associated with wet-spraying of CMA solutions was not examined. The only direct wet-spraying experiments, performed herein, introduced micron-size CMA particles to the furnace. The associated sorbent utilizations were very high, approaching 100%.

Acknowledgments

This work was carried out on U.S. Dept. of Energy University Grants #: DE-FG22-89PC89776 and DE-FG22-92PC92535. We also acknowledge with appreciation the funding of Ms. Zhu with a graduate student stipend provided by the Stone & Webster Engineering Corporation, with special thanks to Dr. Ernest Zabolotny. The authors also acknowledge assistance from Mr. Bill Fowle for SEM microscopy and from Mr. Alan Yen for EDS and XRD analysis.

Literature Cited

Amrnhein, G. T., P. V. Smith, S. J. Vecci, and R. J. Batyko, "Pilot-Scale Demonstration of the LIDS System for SO_2 Control of High-Sulfur Coal," Int. Conf. on Coal Utilization and Slurry Technologies, Clearwater, FL (Apr. 28–May 1, 1992).

Bhatia, S. K., and D. D. Perlmutter, "The Effect of Pore Structure on Fluid-Solid Reactions: Application to the SO_2-Lime Reaction," *AIChE J.*, **76**, 226 (1981).

Calvelo, A., and R. E. Cunningham, "Kinetics of Gas-Solid Reactions. Influence of Surface Area and Effective Diffusivity Profiles," *J. Catal.*, **17**, 1 (1970).

Borgwardt, R. H., N. F. Roache, and K. R. Bruce, "Surface Area of Calcium Oxide and Kinetics of Calcium Sulfide Formation," *Env. Prog.*, **3**, 129 (1984).

Borgwardt, R. H., "Calcination Kinetics and Surface Area of Dispersed Limestone Particles," *AIChE J.*, **31**(1), 103 (1985).

Borgwardt, R. H., "Sintering of Nascent Calcium-Oxide," *Chem. Eng. Sci.*, **44**(1), 53 (1989).

Bortz, S. J., V. P. Roman, and R. J. Yang, "Precalcination and its Effect on Sorbent Utilization during Upper Furnace Injection," Paper 21, *Proceedings: 1986 Joint Symposium on Dry SO_2 and*

Simultaneous SO_2/NO_x Control Technologies, 1, EPRI CS-4966 (Dec., 1986).

Bruce, K. R., B. K. Gullet, and L. O. Beach, "Comparative SO_2 Reactivity of CaO Derived from $CaCO_3$ and $Ca(OH)_2$," *AIChE J.*, **35**(1), 37 (1989).

Bungay, H. H., and L. W. Hudson, "Calcium Magnesium Acetate from Biomass," in *Biomass Conversion Technology: Principles and Practice*, M. Moo-Young, J. C. Lamptey, B. R. Glick, and H. R. Bungay, eds., Pergamon Press (1987).

Case, P. L., M. P. Heap, C. N. McKinnon, D. W. Pershing, and R. Payne, "The Capture and Retention of Sulfur Species by Calcium Compounds during the Combustion of Pulverized Coal," *Amer. Chem. Soc. Div. Fuel Chem. Prepr.*, **27**(1), 158 (1982).

Chang, K. K., R. C. Flagan, G. R. Gavalas, and P. K. Sharma, "Combustion of Calcium-Exchanged Coals," *Fuel*, **65**, 75 (1986).

Cole, J. A., W. R. Kramlich, and G. D. Silcox, "Fundamental Studies of Sorbent Reactivity in Isothermal Reactors," Paper 16, *Proceedings: Joint Symp. on Dry SO_2 and Simultaneous SO_2/NO_x Control Technologies*, 1, EPRI CS-4966 (Dec., 1986).

Cumper, J. G., Y. A. Levendis, and M. Metghalchi, "Characterization of the Environment in a Laminar Flow Furnace with Applications to the Combustion of Coal and Coal-Water Slurries," *Symp. on Heat and Mass Transfer in Fire and Combustion Systems*, ASME Winter Annual Meeting, Dallas (Nov. 25-30, 1990).

Flagan, R. C., and J. H. Seinfeld, *Fundamentals of Air Pollution Engineering*, Prentice Hall, Englewood Cliffs, NJ (1988).

Garman, R. M., and Z. A. Munir, "Surface Area Reduction during Isothermal Sintering," *J. Amer. Ceram. Soc.*, **59**, 379 (1976).

Gullet, B. K., and K. R. Bruce, "Pore Distribution Changes of Calcium-Based Sorbents Reacting with Sulfur Dioxide," *AIChE J.*, **33**, 1719 (1987).

Ibarra, J. V., J. M. Palacios, and A. M. de Andrès, "Analysis of Coal and Char Ashes and Their Ability for Sulphur Retention," *Fuel*, **68**, 861 (1989).

Levendis, Y. A., and R. C. Flagan, "Synthesis, Formation and Characterization of Micron-Sized Glassy Carbon Spheres of Controlled Pore Structure," *Carbon*, **27**(2), 265 (1989a).

Levendis, Y. A., S. W. Nam, M. Loewenberg, R. C. Flagan, and G. R. Gavalas, "Catalysis of the Combustion of Synthetic Char Particles by Various Forms of Calcium Additives," *J. of Energy and Fuels*, **3**, 28 (1989b).

Lindner, B., and D. Simonson, "Comparison of Structural Models for Gas-Solid Reactions in Porous Solids Undergoing Structural Changes," *Chem. Eng. Sci.*, **36**, 1519 (1981).

Lynch, D. C., and J. F. Elliot, "Kinetic of the Oxidation of CaS," *Metall. Trans.*, **9B**, 691 (1978).

Muzio, L. J., and J. K. Arand, "Bench-Scale Study of the Dry Removal of SO_2 with Nacholite and Trona," EPRI CS-1744 (March, 1981).

Panagiotou, T., and Y. A. Levendis, "Generation of Spherical and Monodisperse Particles of Poly(styrene) and Poly(methyl methacrylate) by Atomization of Monomers or Dissolved Polymer Precursors," *J. of Appl. Polym. Sci.*, **43**, 1549 (1991).

Sharma, P. K., G. R. Gavalas, and R. C. Flagan, "Calcium Pretreatment of Coal for Sulphur Emissions Control in Combustion," *Fuel*, **66**, 207 (1987).

Simons, G. A., and A. R. Garman, "Small-Pore Closure and the Deactivation of the Limestone Sulfation Reaction," *AIChE J.*, **32**, 1491 (1986).

Simons, G. A., A. R. Garman, and Boni, A. A., "The Kinetic Rate of SO_2 Sorption by CaO," *AIChE J.*, **33**, 211 (1987).

Simons, G. A., D. O. Ham, T. E. Parker, J. R. Morency, G. Moniz, and A. A. Boni, "Alternative SO_2 Sorbents," Final Report PSI-538 TR-744, Physical Sciences Inc., Andover, MA (1987).

Simons, G. A., "Parameters Limiting Sulfation by CaO," *AIChE J.*, **34**, 167 (1988).

Slack, A. V., and G. A. Hollinden, *Sulfur Dioxide Removal from Waste Gases*, Noyes Data Corp., London (1975).

Sohn, H. Y., and J. Szekely, "A Structural Model for Gas-Solid Reactions with Moving Boundary—III," *Chem. Eng. Sci.*, **27**, 763 (1972).

Sohn, H. Y., and J. Szekely, "A Structural Model for Gas-Solid Reactions with Moving Boundary—IV," *Chem. Eng. Sci.*, **28**, 1169 (1973).

Sotirchos, S. V., "On a Class of Random Pore and Grain Models for Gas-Solid Reactions," *Chem. Eng. Sci.*, **42**, 1262 (1987).

Sotirchos, S. V., and H. C. Yu, "Overlapping Grain Models for Gas-Solid Reactions with Solid Product," *Ind. Eng. Chem. Res.*, **27**, 836 (1988).

Stouffer, M. R., and H. Yoon, "An Investigation of CaO Sulfation Mechanisms in Boiler Sorbent Injection," *AIChE J.*, **35**, 1253 (1989).

Szekely, J., and J. W. Evans, "A Structural Model for Gas-Solid Reactions with a Moving Boundary," *Chem. Eng. Sci.*, **25**, 1091 (1970).

Szekely, J., and J. W. Evans, "A Structural Model for Gas-Solid Reactions with a Moving Boundary—II," *Chem. Eng. Sci.*, **26**, 1901 (1971).

Szekely, J., and M. Propster, "A Structural Model for Gas-Solid Reactions with a Moving Boundary—VI," *Chem. Eng. Sci.*, **30**, 1049 (1975).

Togan, M. A., T. Paloposki, J. D. Teare, J. M. Beér, M. Rini, R. C. LaFlesh, and L. E. Barta, "An Experimental Investigation of Sulfur Capture in Coal-Water Fuel Flames," Int. Conf. on Coal and Slurry Technology (1989).

Torres-Ordoñez, R. J., J. P. Longwell, and A. F. Sarofim, "Intrinsic Kinetics of CaS(s)," *Energy & Fuels*, **3**, 506 (1989).

Tullin, C., and E. Ljungström, "Reaction Between Calcium Carbonate and Sulfur Dioxide," *Energy & Fuels*, **3**, 284 (1989).

Yortsos, Y. C., and M. Sharma, "Application of Percolation Theory to Noncatalytic Gas-Solid Reactions," AIChE Meeting, San Francisco (1984).

Yu, H. C., and S. V. Sotirchos, "A Generalized Pore Model for Gas-Solid Reactions with Pore Closure Behavior," *AIChE J.*, **33**, 382 (1987).

Wise, D. L., and D. Augenstein, "An Evaluation of the Bioconversion of Woody Biomass to Calcium Acetate Deicing Salt," *Solar Energy*, **41**, 453 (1988).

Wise, D. L., Y. A. Levendis, and M. Metghalchi, eds., *Calcium Magnesium Acetate An Emerging Bulk Chemical for Environmental Applications*, Elsevier Science Publishers, Amsterdam (1991).

Manuscript received Feb. 26, 1992, and revision received Oct. 21, 1992.